Abnormal Movement Behavior of Skyrmion in a Circular-ring Nanotrack

Na Cai , Xin Zhang , Yong Hu * , Yan Liu *

Posted Date: 1 November 2023

doi: 10.20944/preprints202311.0052.v1

Keywords: skyrmion; circular ring nanotrack; skyrmion Hall effect; Dzyaloshinskii–Moriya interaction

Article

Abnormal Movement Behavior of Skyrmion in a Circular-Ring Nanotrack

Na Cai, Xin Zhang, Yong Hu * and Yan Liu *

College of Sciences, Northeastern University, Shenyang 110819, People's Republic of China
* Correspondence: liuyanphys@mail.neu.edu.cn, huyong@mail.neu.edu.cn

Abstract: As an outstanding information carrier, skyrmion is increasingly widely used in devices based on complex geometries. To achieve the skyrmion-based spintronic devices, a reasonable and feasible nanotrack is essential. In this paper, we conducted a study on the current-driven skyrmion movement in a circular-ring-shaped nanotrack. Our results suggest that the asymmetry of the inside and outside boundary of the circular ring changed the stable position of the skyrmion, causing it to move like the skyrmion Hall effect when driven by currents. Moreover, the asymmetric boundaries have advantages in enhancing or weakening the skyrmion Hall effect. Additionally, we also compared the skyrmion Hall effect from the asymmetric boundary of circular ring nanotracks with that from inhomogeneous DMI. It is found that the skyrmion Hall effect caused by the circular ring is significantly greater than that caused by the inhomogeneous DMI. These results contribute to our understanding of the skyrmion dynamics in confined geometries and offer an alternative method for controlling the skyrmion Hall effect of skyrmion-based devices.

Keywords: skyrmion; circular ring nanotrack; skyrmion Hall effect; Dzyaloshinskii–Moriya interaction

1. Introduction

Skyrmion is a fascinating particle-like swirling spin configuration that has garnered significant attention since its inception [1,2]. Its topological properties make it incredibly stable and endow it with exotic particle dynamics behavior [3–5]. Moreover, the successful experimental observation and controllability of skyrmion in a wide temperature range and near zero field opened the door for their application in spintronic devices [6–13]. Due to their topological stability, low driving current, and small size, skyrmions are expected to further enhance the performance of spin electronic devices [14–18]. In other words, the development of skyrmion-based devices is expected to further improve the current storage capacity of information.

It is well known that when driven by the current, the skyrmion Hall effect (SkHE) causes skyrmions to drift away from the driving current direction [19,20]. The processing of SkHE is one crucial factor in the advancement of skyrmion-based devices. In the past, SkHE was viewed as a harmful problem for devices, so great efforts have been made to suppress it [21–23]. However, in recent times, SkHE has been intensively explored by researchers who have created several devices based on it [20,24–29]. For example, Whang *et al.* proposed a fast and robust oscillator that utilizes SkHE to modulate the skyrmion's movement [26]. Hong *et al*. designed transistors by capitalizing on the large transverse motion of skyrmions induced by SkHE [24]. Moreover, researchers have proposed and implemented diodes by utilizing the SkHE-induced skyrmion unidirectional transport [29–31]. That is to say, the SkHE can control the movement of the skyrmion when it performs different functions of the devices.

Apart from controlling SkHE, the effect of nanotrack boundaries on the skyrmion movement can also not be disregarded in skyrmion-based devices. Studies have indicated that the nanotrack's boundaries can significantly impact skyrmions' behavior [17,29,32–38]. According to a study by Saidi et al., when nearing the edge of the track, the skyrmions shrink in size and follow a spiral path [34]. Another research by Morshed et al. has revealed that the boundary with notches has a notable pinning influence on the skyrmion[38]. Inspired by this motivation, we investigate the current-driven

 doi:10.20944/preprints202311.0052.v1

behavior of skyrmion in circular ring-shaped nanotracks. Compared with the symmetrical straight nanotrack, the inner and outer boundaries of the ring are asymmetric, which may bring some abnormal phenomena.

2. Materials and Methods

We modeled ultra-thin ferromagnetic Co/Pt with a circular ring nanotrack shown in Figure 1(a), which can be experimentally fabricated by lithography techniques [39,40]. Our simulations were carried out by using the mumax3 software package [41,42]. The circular ring nanotrack was parametrized as: $\boldsymbol{\gamma} = R_{\mathrm{m}} \cdot (\boldsymbol{e}_x \cos\theta + \boldsymbol{e}_y \sin\theta)$, where R_{m} is the middle line radius of the tracks, ($\boldsymbol{e}_x$, $\boldsymbol{e}_y$) is the Cartesian basis. During our simulation, the track was discretized into small discretization cells with the size of 2×2×h nm^3, where h represents the thickness of the track. We first initialized a Neél type skyrmion at the initial center of the track and then injected an in-plane current to drive the skyrmion moving along the circular ring nanotrack. In experiments, skyrmion can be produced by electric pulse, local heating, magnetic field, and other methods [43,44]. The red and black arrows in Figure 1(a) represent the clockwise (CW) and counterclockwise (CCW) directions of the current, which are both equally dispersed across the circular ring. We refer to the situation of the skyrmion traveling clockwise in the full text as CW, and the case of the skyrmion traveling counterclockwise as CCW.

The time-dependent magnetization dynamics driven by an in-plane current is governed by the Laudau–Lifshitz–Gilbert equation containing the spin-transfer torque (STT) effect:

$$\dot{\mathbf{m}} = -\gamma \mathbf{m} \times \mathbf{H}_{eff} + \alpha (\mathbf{m} \times \dot{\mathbf{m}}) + \mathbf{m} \times [\mathbf{m} \times (\boldsymbol{u} \cdot \nabla)\mathbf{m}] + \beta \mathbf{m} \times (\boldsymbol{u} \cdot \nabla)\mathbf{m}. \quad (1)$$

where $\mathbf{m}$=M/M_{s} is the normalized magnetization vector, M_{s} is the saturation magnetization. The effective magnetic field is given by $\mathbf{H}_{eff} = -(\delta E / \delta \mathbf{m})/\mu_0 M_{\mathrm{s}}$, where μ_0 is the vacuum permeability, and E is the magnetic energy of the system, including energy terms such as exchange, anisotropy, DMI, Zeeman, and demagnetization energy. The interfacial DMI energy density is given by $E_{\mathrm{DM}} = -D_{\mathrm{M}} \mathbf{m} \cdot ((\hat{\mathbf{z}} \times \nabla) \times \mathbf{m})$, where D_{M} is the DMI constant. For $\mu = \mu_B jp / eM_{\mathrm{s}}$, where j is the current density, p is the spin polarization rate, μ_B is Bohr magneton, and $\boldsymbol{e}$ is the electron charge. α and β are the Gilbert damping constant and the non-adiabaticity factor, respectively. We choose the case $\alpha = \beta = 0.01$ here to exclude the intrinsic SkHE [45]. The magnetic parameters we use here are as follows: $M_{\mathrm{s}} = 5.8\times10^5\ \mathrm{A\cdot m^{-1}}$, $A = 15\times10^{-12}\ \mathrm{J\cdot m^{-1}}$, $D_{\mathrm{M}} = 3\times10^{-3}\ \mathrm{J\cdot m^{-2}}$, $K_{\mathrm{u}} = 8\times10^5\ \mathrm{J\cdot m^{-3}}$, $p = 0.5$.

3. Results

The function between skyrmion velocity and the position in the circular ring nanotrack enables us to determine the dynamics of skyrmion. We calculate the skyrmion velocity and decompose it into two components, parallel velocity $V_{\parallel}$ and perpendicular velocity $V_{\perp}$, where $V_{\parallel}$ ($V_{\perp}$) is the velocity component along(perpendicular) the current direction. The positive directions of $V_{\parallel}$ and $V_{\perp}$ are along $\boldsymbol{e}_{\mathrm{T}}$ and $\boldsymbol{e}_{\mathrm{N}}$, respectively. It can be seen from Figure 1(b) that $V_{\parallel}$ shows a periodic trend of increasing first and then decreasing in both CCW and CW directions, where $V_{\parallel}$ of CCW (CW) with Q=-1 overlaps with CW(CCW) with Q=1. This fluctuation also occurs in $V_{\perp}$, as shown in Figure 1(c), which fluctuates over a non-zero value and has the same periodicity as $V_{\parallel}$. This fluctuation of velocity is significantly different from the case in a straight track. In a straight track, the velocity remains constant in parallel and zero in perpendicular direction for $\alpha = \beta$. However, in a circular ring nanotrack, the velocity fluctuates significantly. To compare the movement behavior of a skyrmion in both tracks, we define R_{sk} as the radius of the real moving trajectory and R_{m} as the radius of the middle line of the circular ring. Here we let $R_{\mathrm{d}} = R_{\mathrm{m}} - R_{\mathrm{sk}}$, which is the distance between the middle line and the real moving trajectory. Figure 1(d) shows the variation of R_{d} with the angle position. The initial non-zero value of R_{d} indicates that the skyrmion undergoes a transverse drift from the middle line. It means that the

Preprints (www.preprints.org) | NOT PEER-REVIEWED | Posted: 1 November 2023 doi:10.20944/preprints202311.0052.v1

skyrmion initially stabilizes inside the middle line and then moves towards the inner or outer boundary of the track driven by the current flow.

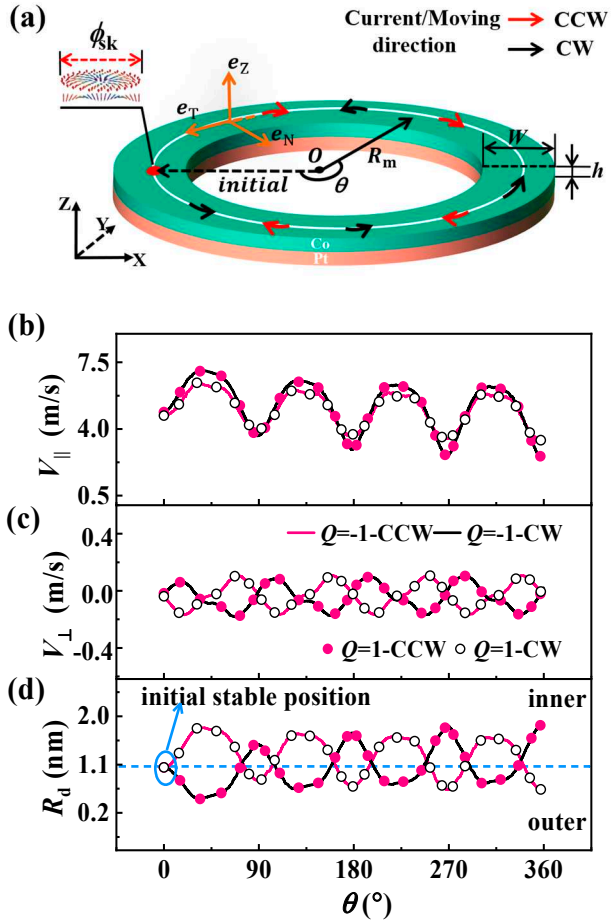

Figure 1. Model and the skyrmion dynamics. **(a)** The schematic of the circular ring nanotrack, where θ represents the angular parameter of skyrmion at different positions, and Rm is the middle line radius of the tracks. The red arrows and black arrows represent the clockwise (CCW) and counterclockwise (CW) driving current (moving) directions respectively. **(b)** The parallel velocity $V_{\parallel}$, perpendicular velocity $V_{\perp}$ **(c)**, and the drift distance of the initial stable position **(d)** as functions of the position parameter θ. Q represents the topological number of skyrmion.

Upon observing skyrmion movement in the circular ring nanotrack, we found that the skyrmion moves at a certain angle relative to the driving current, similar to the drift caused by the skyrmion Hall effect (SkHE). We so calculate the Hall angle θ_{SkHE} of the skyrmion in a circular ring track and show it in Figure 2(a), where $\theta_{\mathrm{SkHE}} = \arctan(V_{\perp}/V_{\parallel})$. It is evident that the circular ring nanotrack exhibits a non-zero Hall angle, with a maximum value of about 2°. We discovered that this type of SkHE still exists when the track thickness is changed to h=0.4 nm and h=1 nm, and it is not affected by the thickness of the circular track. In traditional SkHE, the skyrmion topological number Q and the movement direction are the key factors affecting the process, as shown in the gray section of Figure 2(a). Similar to the traditional SkHE, the Hall angle also demonstrates a notable reliance on the direction of motion and the skyrmion topological number Q in a circular ring nanotrack. For a skyrmion with Q=-1, a CCW current drives it towards the inner side, while the CW current drives it towards the outer side of the circular ring nanotrack. The situation is exactly the opposite for a skyrmion with Q=1.

Preprints (www.preprints.org) | NOT PEER-REVIEWED | Posted: 1 November 2023 doi:10.20944/preprints202311.0052.v1

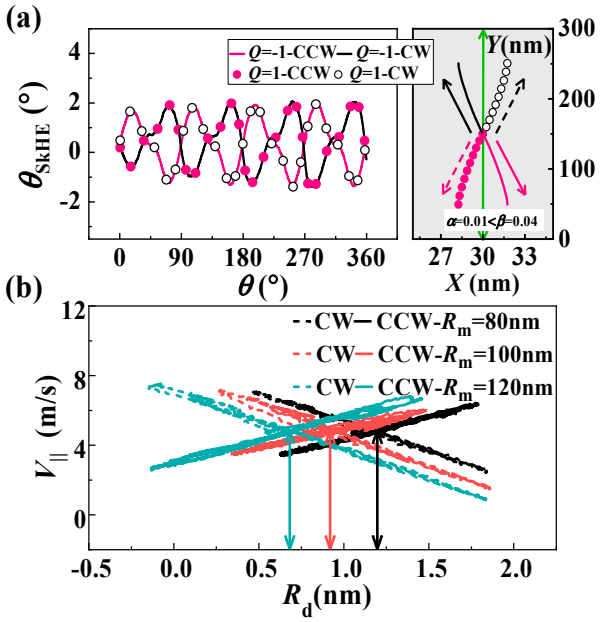

Figure 2. Skyrmion dynamics in the circular ring. **(a)** The skyrmion Hall angle as function of the position parameter θ. The gray part shows the trajectories of skyrmion under the conventional skyrmion Hall effect for the case $\alpha < \beta$. **(b)** The function between $V_{\parallel}$ and the drift distance R_d for different middle line radius R_m values. Unless otherwise specified, the simulations were carried out under the fixed width W=60 nm and the applied current density $j = 1\times10^{11}\ \mathrm{A\cdot m^{-2}}$.

Based on the obtained results, it can be concluded that the movement of skyrmion in circular ring nanotracks is similar to SkHE. However, SkHE does not occur in the straight nanotrack when $\alpha = \beta$. This leads us to assume that the SkHE observed in circular rings may be due to the asymmetry inner and outer boundaries of the circular ring. In Figure 2(b), we show the variation of $V_{\parallel}$ with the drift distance R_d for different R_m. It can be found that $V_{\parallel}$ are linearly related to R_d in both directions, it is just a negative correlation in CW and a positive correlation in CCW. The situations of Q=1 are the opposite. Furthermore, special attention should be paid to the fact that the stable positions of the skyrmion, represented by the intersection of the velocities in two directions, are significantly different for circular ring nanotracks with different sizes. The stable position of a skyrmion is directly influenced by the size of the circular ring nanotrack. As the size of the ring decreases, its curvature becomes more prominent, leading to reduced symmetry between its inner and outer boundaries. Conversely, larger circular rings appear more symmetrical with a smaller difference between the inner and outer boundaries. Due to the asymmetric boundary of the circular ring nanotrack, the stable position of the skyrmion drifts farther from the middle line as the circular ring nanotrack size decreases. When a skyrmion moves along a straight track, it remains stable on the centerline without deviation for a certain distance. However, when a skyrmion moves along a curved track, the collision of the skyrmion with the asymmetric boundaries of the track results in periodic changes in the skyrmion's Hall angle. This, in turn, leads to periodic increases and decreases in velocity. Therefore, the period of such collisions is uncertain. When we modify the size of the nanotrack or the driving current density, the SkHE still exhibits an oscillation mode, but the period changes accordingly.

To deeply understand the influence of asymmetric boundaries on the movement of the skyrmion in the circular ring nanotrack, the Thiele equation is used. Since the size of skyrmion changes is not obvious and the topological structure and stability are maintained, we still treat the skyrmion as a rigid object in asymmetric track. This rigid approximation allows the Thiele equation for the skyrmion is written as:

$$\boldsymbol{G}\times(\mathbf{V}^{e}-\mathbf{V}^{sk})+D(\beta\mathbf{V}^{e}-\alpha\mathbf{V}^{sk})-\nabla U=\mathbf{0}, \tag{2}$$

Preprints (www.preprints.org) | NOT PEER-REVIEWED | Posted: 1 November 2023 doi:10.20944/preprints202311.0052.v1

where the first term is the Magnus force, **G** is the gyrovector related to the topological number Q of skyrmion, and **G**=(0, 0, 4πQ) is a constant for Néel skyrmion. The second term of Eq. (2) stands for the dissipative force and the D comes from a dimensionless matrix related to the dissipative force, being its components D_{xx}=D_{yy}=D. $\mathbf{V}^{e}=(V^{e},0)=(-Pl^{3}\mathbf{j}/2eM_{s},0)$ is the velocity of the electron, and l is the lattice constant of the material. The $\mathbf{V}^{\mathrm{sk}}=(V_{\parallel},V_{\perp})$ is the velocity of skyrmion that can be decomposed into two orthogonal parts (the tangential and radial directions of the circular-ring nanotrack). The third term $-\nabla U$ represents the force acting on the moving skyrmion and $\mathbf{F}=(F_{\mathrm{T}},F_{\mathrm{N}})$, including the forces from the boundary and driving current.

For $\alpha=\beta$, we can get the simplification form of skyrmion velocity from Eq. (2):

$$V^{\mathrm{sk}}=\begin{pmatrix}V_{\parallel}\\V_{\perp}\end{pmatrix}=\frac{1}{G^{2}+\alpha^{2}D^{2}}\begin{pmatrix}(G^{2}+\alpha^{2}D^{2})V^{e}+\alpha DF_{\mathrm{T}}+GF_{\mathrm{N}}\\-GF_{\mathrm{T}}+\alpha DF_{\mathrm{N}}\end{pmatrix} \tag{3}$$

Considering D=|G| and $\alpha\ll 1$ ($\alpha^{2}+1\approx 1$) the function of velocity can be further simplified as:

$$\begin{aligned}V_{\parallel}&=V^{e}+\frac{\alpha F_{\mathrm{T}}}{D}-\frac{F_{\mathrm{N}}}{G}\\V_{\perp}&=\frac{\alpha F_{\mathrm{N}}}{D}+\frac{F_{\mathrm{T}}}{G}\end{aligned} \tag{4}$$

It can be concluded from Eq. (4) that the $V_{\parallel}$ is determined by the sign of V^{e} and the product of G (Q) and F_{N}. The force F_{N} acting on the skyrmion mainly comes from the repulsive force from the boundary, it is negative when the skyrmion moves towards the inner boundary and positive when the skyrmion moves towards the outer boundary. When a skyrmion with Q=-1 moves in a counterclockwise direction and approaches the inner boundary, its velocity increases. However, when it approaches the outer boundary, its velocity decelerates. For skyrmions with Q=+1, the situation is the opposite since G is positive. This is consistent with the variations in skyrmion velocity described in Figure 1(b).

The SkHE caused by the asymmetry of the inner and outer boundaries is also reflected in the drift in the skyrmion stable. We so calculated the relationship between the initial drift distance R_{d} and the radius R_{m} of the circular ring nanotrack under a range of values $\alpha(\beta)$. The results, as shown in Figure 3(a), revealed that the skyrmion's stable position tends to drift further away from the middle line as the size of the circular ring decreases. As shown in the inset of Fig.3(a), even if the values $\alpha(\beta)$ are different, R_{d} is linearly correlated with the curvature $\kappa=R_{\mathrm{m}}^{-1}$ of the nanotrack. Because the symmetry of the boundary is directly affected by the curvature of the circular ring. Additionally, both Figure 3(a) and the illustration in it show that the dependence of skyrmion size ϕ_{sk} (the red line) on the R_{m} is the same as that of R_{d}. Essentially, the force from the asymmetric boundary changes the size of the skyrmion and thus changes its stable position on the track.

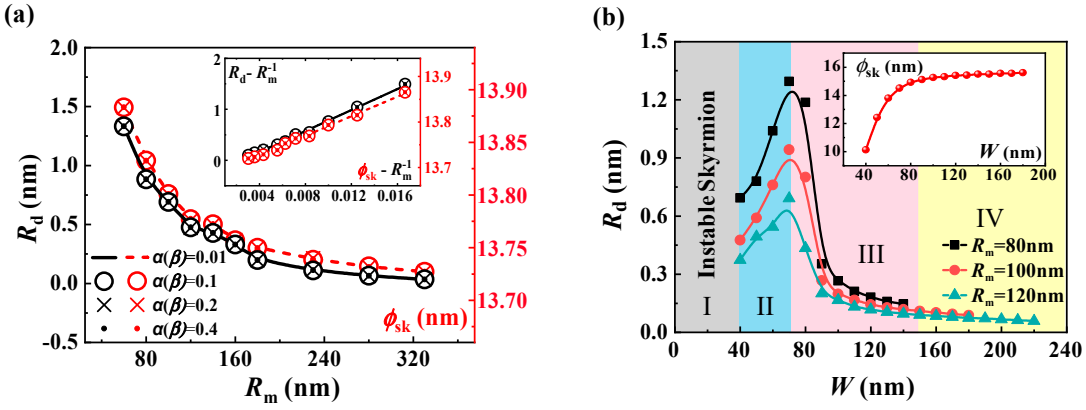

Figure 3. The analysis of skyrmion dynamics. **(a)**The drift distance R_{d} (black line) and the size of skyrmion ϕ_{sk} (red line) as functions of the middle line radius R_{m} for the cases of no current and

Preprints (www.preprints.org) | NOT PEER-REVIEWED | Posted: 1 November 2023 doi:10.20944/preprints202311.0052.v1

different $\alpha(\beta)$ values. **(b)** The drift distance R_d as a function of track width W, where the R_m is fixed at 80 nm, 100 nm, and 120 nm respectively. Unstable region II, width dominant region II, asymmetric boundaries dominant region III, low response region IV.

In addition to the size R_m of the circular ring nanotrack, the width also affects the force exerted by the boundary on skyrmion [46,47]. Figure 3(b) illustrates the drift distance R_d changes with the track's width when the R_m is fixed at 80 nm, 100 nm, and 120 nm. Generally, it is still true that the smaller the R_m, the more obvious the skyrmion stable state drift from the initial position. However, for the same R_m values, the stable state can be divided into four regions at different width values, as shown in Figure 3(b). In region I ($0<W<40$ nm), the tracks are too narrow for a stable skyrmion. In region II ($40<W<70$ nm), although the asymmetric boundary reduces the size of the skyrmion, the increase in width significantly increases the size of the skyrmion, causing R_d to gradually increase until the increase in width has little effect on the size of skyrmion. When $W>70$ nm, the skyrmion size does not increase significantly, so the R_d in region III and IV is consistent with the effect of the size of a circular ring. For larger W in region IV ($W>140$nm), the corresponding $R_d \leq 0.15$ nm and the asymmetric boundary drift can be almost ignored. This is because as the track becomes wider, although the force caused by the asymmetric boundary still exists because the boundary is too far away from the skyrmion, the stable position will hardly move much.

In order to confirm our analysis, we also calculate the skyrmion velocity on a wider nanotrack. Our findings reveal that as the track width is very wide, the periodic oscillation of $V_{\parallel}$ (depicted in Figure 1(b)) diminishes or entirely disappears, and $V_{\perp}$ (depicted in Figure 1(c)) comes close to zero. To verify this, we tested the case of a width of W=150 nm. As shown in Figure 4(a) and (b), $V_{\parallel}$ no longer displays an obvious fluctuation, but remains close to the velocity in the long straight track, and $V_{\perp}$ is also close to zero, as expected. The reason for this is for a fixed R_m, the boundary's symmetry for the skyrmion's stable position remains the same. However, the repulsive force from the boundary weakens as the track gets wider. This force is related to the size of the skyrmion and its distance from the boundary. As a result, the skyrmion remains unaffected by the boundary.

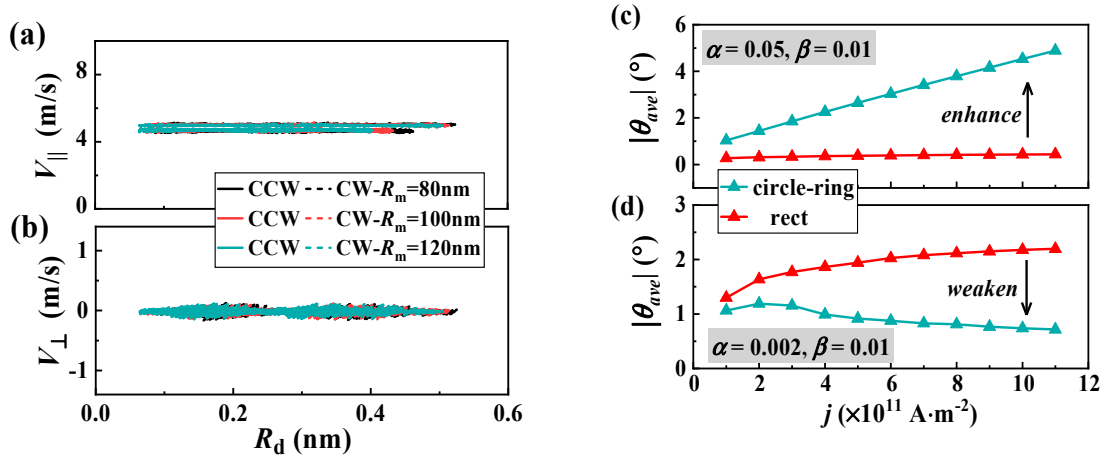

Figure 4. Verification of the skyrmion dynamics. The skyrmion velocity **(a)** parallel velocity $V_{\parallel}$ and **(b)** perpendicular velocity $V_{\perp}$ as functions of its position parameter θ with different middle line radius R_m when the width is fixed at 150 nm. The average values of the Hall angle as functions of the current density in circular ring nanotrack and straight track for the cases of **(c)** $\alpha > \beta$ and **(d)** $\alpha < \beta$.

Since the asymmetric inner and outer boundaries of a circular ring can generate the SkHE, we have also studied the impact of asymmetric boundaries on the circular rings that already have the SkHE. As illustrated in Figure 4(c) and (d), when $\alpha > \beta$ the Hall angle in a circular ring track is greater than that in a straight track, the SkHE is enhanced. On the other hand, when $\alpha < \beta$ the Hall angle in the circular ring nanotrack is smaller than that in a straight track, the SkHE is weakened. Therefore,

Preprints (www.preprints.org) | NOT PEER-REVIEWED | Posted: 1 November 2023 doi:10.20944/preprints202311.0052.v1

the asymmetric boundaries may be used to strengthen or weaken the SkHE. That is utilizing a circular ring nanotrack offers a promising way to manipulate the SkHE in devices.

According to research, SkHE can also be induced by inhomogeneous DMI [48]. In this section, we compared the effect of asymmetric boundary with that of inhomogeneous DMI. We created straight nanotracks with inhomogeneous DMI, which had the same width as the circular ring nanotracks. Firstly, we compared the effect of non-uniform DMI on the skyrmion's stable position with the circular ring. The graph in Figure 5(a) illustrates the relationship between the DMI change values and the drifted distance of the skyrmion's stable position for different initial DMI values. When there was no change in DMI, the skyrmion stayed in the center of the track. However, when there was a slight DMI change, the skyrmion drifted from its middle line. The 1.25×10^{-6} $J\cdot m^{-2}$ / nm DMI gradient in can cause a similar drift distance of the skyrmion's stable position with the circular ring with R_m=80 nm.

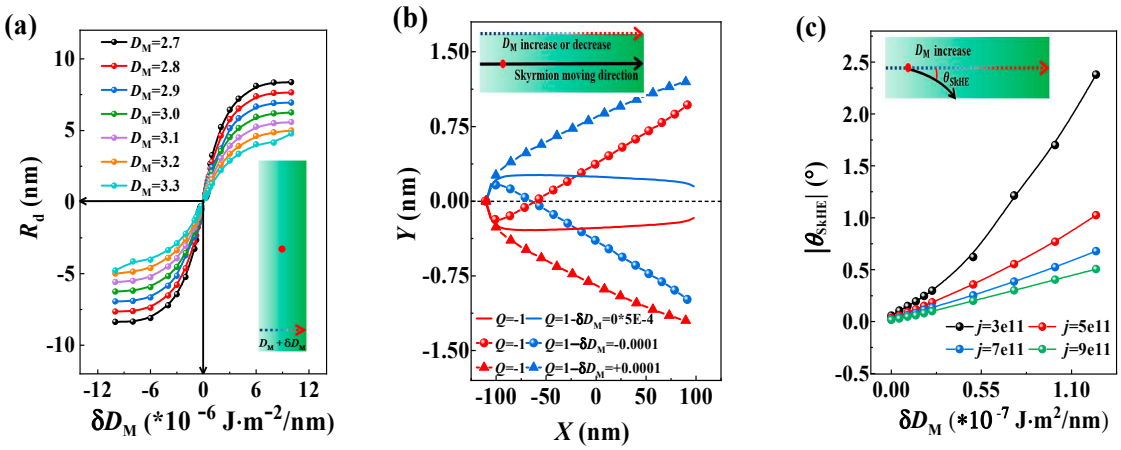

Figure 5. Skyrmion dynamics in an inhomogeneous DMI distribution nanotrack. **(a)** The drift distance R_d as a function of the DMI change value in long straight tracks for different initial DMI values. **(b)** Skyrmion motion trajectory driven by the current in the modeled nanotrack, where the modeled track with an inhomogeneous DMI distribution in the long direction. **(c)** The Hall angle as a function of the DMI change value in the modeled nanotrack.

We also conducted an analysis to determine the factors that influence the Hall angle in the inhomogeneous DMI distribution tracks. The trajectory of the skyrmion in the modeled nanotrack is shown in Figure 5(b). It was observed that the presence of an inhomogeneous DMI distribution in the nanotrack causes the skyrmion to move toward the boundaries as it moves in a circular ring. Additionally, we found that the sign of the Hall angle depends on the sign of δ_{D_M} and skyrmion topological number Q. Figure 5(c) illustrates the relationship between the Hall angle and the value of the DM changes value for various current densities. Compared with the circular ring, 1.1×10^{-7} $J\cdot m^{-2}$ / nm DMI gradient can only yield a Hall angle of about 2° for j =3.0×10^{-3} $A\cdot m^{-2}$ driving current. For high current density, a larger DMI gradient is required to cause a 2° Hall angle. Therefore, the SkHE caused by the circular ring is much more significant than that caused by the inhomogeneous DMI.

4. Conclusions

In conclusion, we investigate the current-driven skyrmion movement in circular-ring-shaped nanotracks. The result shows that the presence of an asymmetric boundary causes the shift of the skyrmion's stable position, leading the skyrmion to move like the skyrmion Hall effect when driven by current. We also notice that the skyrmion velocity can be linearly changed by the skyrmion Hall effect induced by the asymmetric boundary of the circular ring nanotrack. The asymmetric boundaries also have advantages in enhancing or weakening the skyrmion Hall effect. We also compared the skyrmion Hall effect from the asymmetric boundary of circular ring nanotracks with

that from inhomogeneous DMI. It is found that the skyrmion Hall effect caused by the circular ring is significantly greater than that caused by the inhomogeneous DMI. These findings not only contribute to our understanding of the dynamics of skyrmions in confined geometries but also provide an alternative approach to controlling the skyrmion Hall effect of skyrmion-based devices.

Author Contributions: Conceptualization, N.C., Y.H. and Y.L.; Methodology, N.C., Y.H. and Y.L.; Software, N.C., X.Z., Y.H. and Y.L.; Validation, N.C., Y.H. and Y.L.; Formal analysis, N.C., Y.H. and Y.L.; Investigation, N.C., Y.H. and Y.L.; Resources, N.C., X.Z., Y.H. and Y.L.; Writing—original draft, N.C. Y.H. and Y.L.; Supervision, Y.H. and Y.L.; Project administration, Y.H. and Y.L.; Funding acquisition, Y.H. and Y.L. All authors have read and agreed to the published version of the manuscript.

Funding: This work was supported by the LiaoNing Revitalization Talents Program (Grant No. XLYC2007150), the Fundamental Research Funds for the Central Universities of Ministry of Education of China (N2205015), and the National Natural Science Foundation of China (Grant No. 11774045).

Data Availability Statement: All the data present in this paper will be made available upon reasonable request. Please contact the corresponding author for further information.

Conflicts of Interest: The authors declare no conflict of interest.

References

1. Rossler, U.K.; Bogdanov, A.N.; Pfleiderer, C. Spontaneous skyrmion ground states in magnetic metals. *Nature*, **2006**, 442, 797.
2. Nagaosa, N.; Tokura, Y. Topological properties and dynamics of magnetic skyrmions. *Nat. Nanotechnol.*, **2013**, 8(12), 899.
3. Kravchuk, V.P.; Rossler, U.K.; Volkov, O.M.; Sheka, D.D.; van den Brink, J.; Makarov, D.; Fuchs, H.; Fangohr, H.; Gaididei, Y. Topologically stable magnetization states on a spherical shell: Curvature-stabilized skyrmions. *Phys. Rev. B*, **2016**, 94(14), 144402.
4. Wang, W.; Song, D.; Wei, W.; Nan, P.; Zhang, S.; Ge, B.; Tian, M.; Zang, J.; Du, H. Electrical manipulation of skyrmions in a chiral magnet. *Nat. Commun.*, **2022**, 13(1).
5. Castillo-Sepúlveda, S.; Vélez, J.A.; Corona, R.M.; Carvalho-Santos, V.L.; Laroze, D.; Altbir, D. Skyrmion dynamics in a double-disk geometry under an electric current. *Nanomaterials*, **2022**, 12(18), 3086.
6. Woo, S.; Litzius, K.; Kruger, B.; Im, M.Y.; Caretta, L.; Richter, K.; Mann, M.; Krone, A.; Reeve, R.M.; Weigand, M.; Agrawal, P.; Lemesh, I.; Mawass, M.A.; Fischer, P.; Klaui, M.; Beach, G.S. Observation of room-temperature magnetic skyrmions and their current-driven dynamics in ultrathin metallic ferromagnets. *Nat. Mater.*, **2016**, 15(5), 501.
7. Boulle, O.; Vogel, J.; Yang, H.; Pizzini, S.; de Souza Chaves, D.; Locatelli, A.; Mentes, T.O.; Sala, A.; Buda-Prejbeanu, L.D.; Klein, O.; Belmeguenai, M.; Roussigne, Y.; Stashkevich, A.; Cherif, S.M.; Aballe, L.; Foerster, M.; Chshiev, M.; Auffret, S.; Miron, I.M.; Gaudin, G. Room-temperature chiral magnetic skyrmions in ultrathin magnetic nanostructures. *Nat. Nanotechnol.*, **2016**, 11(5), 449.
8. Yu, G.; Upadhyaya, P.; Li, X.; Li, W.; Kim, S.K.; Fan, Y.; Wong, K.L.; Tserkovnyak, Y.; Amiri, P.K.; Wang, K.L. Room-Temperature Creation and Spin-Orbit Torque Manipulation of Skyrmions in Thin Films with Engineered Asymmetry. *Nano Lett*, **2016**, 16(3), 1981.
9. Yu, G.; Jenkins, A.; Ma, X.; Razavi, S.A.; He, C.; Yin, G.; Shao, Q.; He, Q.L.; Wu, H.; Li, W.; Jiang, W.; Han, X.; Li, X.; Bleszynski Jayich, A.C.; Amiri, P.K.; Wang, K.L. Room-Temperature Skyrmions in an Antiferromagnet-Based Heterostructure. *Nano Lett*, **2018**, 18(2), 980.
10. Sampaio, J.; Cros, V.; Rohart, S.; Thiaville, A.; Fert, A. Nucleation, stability and current-induced motion of isolated magnetic skyrmions in nanostructures. *Nat. Nanotechnol.*, **2013**, 8(11), 839.
11. Iwasaki, J.; Mochizuki, M.; Nagaosa, N. Current-induced skyrmion dynamics in constricted geometries. *Nat. Nanotechnol.*, **2013**, 8(10), 742.
12. Zhou, Y.; Ezawa, M. A reversible conversion between a skyrmion and a domain-wall pair in a junction geometry. *Nat Commun*, **2014**, 5, 4652.
13. Wang, Y.D.; Wei, Z.J.; Tu, H.R.; Zhang, C.H.; Hou, Z.P. Electric field manipulation of magnetic skyrmions. *Rare Metals*, **2022**, 41(12), 4000.
14. Jonietz, F.; Mühlbauer, S.; Pfleiderer, C.; Neubauer, A.; Munzer, W.; Bauer, A.; Adams, T.; Georgii, R.; Boni, P.; Duine, R.A.; Everschor, K.; Garst, M.; Rosch, A. Spin transfer torques in MnSi at ultralow current densities. *Science*, **2010**, 330(6011), 1648.
15. Fert, A.; Cros, V.; Sampaio, J. Skyrmions on the track. *Nat. Nanotechnol.*, **2013**, 8(3), 152.
16. Yu, X.Z.; Kanazawa, N.; Zhang, W.Z.; Nagai, T.; Hara, T.; Kimoto, K.; Matsui, Y.; Onose, Y.; Tokura, Y. Skyrmion flow near room temperature in an ultralow current density. *Nat. Commun.*, **2012**, 3, 988.

17. Zhang, H.Y.; Zhu, D.Q.; Kang, W.; Zhang, Y.G.; Zhao, W.S. Stochastic computing implemented by skyrmionic logic devices. *Phys. Rev. Appl.*, **2020**, 13(5), 054049.
18. Lin, J.-Q.; Chen, J.-P.; Tan, Z.-Y.; Chen, Y.; Chen, Z.-F.; Li, W.-A.; Gao, X.-S.; Liu, J.-M. Manipulation of skyrmion motion dynamics for logical device application mediated by inhomogeneous magnetic anisotropy. *Nanomaterials*, **2022**, 12(2), 278.
19. Chen, G. Skyrmion Hall effect. *Nat. Phys.*, **2017**, 13(2), 112.
20. Göbel, B.; Mertig, I. Skyrmion ratchet propagation: utilizing the skyrmion Hall effect in AC racetrack storage devices. *Sci. Rep.*, **2021**, 11(1), 3020.
21. Shigenaga, T.; Leonov, A.O. Harnessing skyrmion Hall effect by thickness gradients in wedge-shaped samples of cubic helimagnets. *Nanomaterials*, **2023**, 13(14), 2073.
22. Guo, J.; Hou, Y.; Zhang, X.; Pong, P.W.T.; Zhou, Y. Elimination of the skyrmion Hall effect by tuning perpendicular magnetic anisotropy and spin polarization angle. *Phys. Lett. A*, **2022**, 456, 128497.
23. Zhang, S.F.; Wang, J.B.; Zheng, Q.; Zhu, Q.Y.; Liu, X.Y.; Chen, S.J.; Jin, C.D.; Liu, Q.F.; Jia, C.L.; Xue, D.S. Current-induced magnetic skyrmions oscillator. *New J. Phys.*, **2015**, 17(2), 023061.
24. Hong, I.S.; Lee, K.J. Magnetic skyrmion field-effect transistors. *Appl. Phys. Lett.*, **2019**, 115(7), 072406.
25. Zhou, L.; Qin, R.; Zheng, Y.-Q.; Wang, Y. Skyrmion Hall effect with spatially modulated Dzyaloshinskii–Moriya interaction. *Front. Phys.*, **2019**, 14(5), 536021.
26. Whang, H.S.; Choe, S.B. Spin-Hall-effect-modulation skyrmion oscillator. *Sci Rep*, **2020**, 10(1), 11977.
27. Hu, C.L.; Zhao, R.Z.; Ji, L.Z.; Chen, W.C.; Bandaru, S.; Zhang, X.F. A universal law for predicting the motion behaviors of skyrmions under spatially-varying strain field. *J. Magn. Magn. Mater.*, **2020**, 513, 166954.
28. Tan, A.K.C.; Ho, P.; Lourembam, J.; Huang, L.; Tan, H.K.; Reichhardt, C.J.O.; Reichhardt, C.; Soumyanarayanan, A. Visualizing the strongly reshaped skyrmion Hall effect in multilayer wire devices. *Nat Commun*, **2021**, 12(1), 4252.
29. Feng, Y.; Zhang, X.; Zhao, G.; Xiang, G. A skyrmion diode based on skyrmion Hall effect. *IEEE Trans. Electron Devices*, **2022**, 69(3), 1293.
30. Wang, J.L.; Xia, J.; Zhang, X.C.; Zheng, X.Y.; Li, G.Q.; Chen, L.; Zhou, Y.; Wu, J.; Yin, H.H.; Chantrell, R.; Xu, Y.B. Magnetic skyrmionium diode with a magnetic anisotropy voltage gating. *Appl. Phys. Lett.*, **2020**, 117(20), 202401.
31. Song, C.; Zhao, L.; Liu, J.; Jiang, W. Experimental Realization of a Skyrmion Circulator. *Nano Lett.*, **2022**, 22(23), 9638.
32. Castell-Queralt, J.; González-Gómez, L.; Del-Valle, N.; Sanchez, A.; Navau, C. Accelerating, guiding, and compressing skyrmions by defect rails. *Nanoscale*, **2019**, 11(26), 12589.
33. Yoo, M.-W.; Cros, V.; Kim, J.-V. Current-driven skyrmion expulsion from magnetic nanostrips. *Phys. Rev. B*, **2017**, 95(18).
34. Al Saidi, W.; Sbiaa, R.; Bhatti, S.; Piramanayagam, S.N.; Al Risi, S. Dynamics of interacting skyrmions in magnetic nano-track. *J. Phys. D: Appl. Phys.*, **2023**, 56(35), 355001.
35. Paikaray, B.; Kuchibhotla, M.; Haldar, A.; Murapaka, C. Skyrmion based majority logic gate by voltage controlled magnetic anisotropy in a nanomagnetic device. *Nanotechnology*, **2023**, 34(22), 225202.
36. Shu, Y.; Li, Q.; Xia, J.; Lai, P.; Hou, Z.; Zhao, Y.; Zhang, D.; Zhou, Y.; Liu, X.; Zhao, G. Realization of the skyrmionic logic gates and diodes in the same racetrack with enhanced and modified edges. *Appl. Phys. Lett.*, **2022**, 121(4).
37. Jung, D.-H.; Han, H.-S.; Kim, N.; Kim, G.; Jeong, S.; Lee, S.; Kang, M.; Im, M.-Y.; Lee, K.-S. Magnetic skyrmion diode: Unidirectional skyrmion motion via symmetry breaking of potential energy barriers. *Phys. Rev. B*, **2021**, 104(6), L060408.
38. Morshed, M.G.; Vakili, H.; Ghosh, A.W. Positional Stability of Skyrmions in a Racetrack Memory with Notched Geometry. *Phys. Rev. Appl.*, **2022**, 17(6), 064019.
39. Gaididei, Y.; Kravchuk, V.P.; Sheka, D.D. Curvature effects in thin magnetic shells. *Phys. Rev. Lett.*, **2014**, 112(25), 257203.
40. Streubel, R.; Fischer, P.; Kronast, F.; Kravchuk, V.P.; Sheka, D.D.; Gaididei, Y.; Schmidt, O.G.; Makarov, D. Magnetism in curved geometries. *J. Phys. D: Appl. Phys.*, **2016**, 49(36), 363001.
41. Vansteenkiste, A.; Leliaert, J.; Dvornik, M.; Helsen, M.; Garcia-Sanchez, F.; Van Waeyenberge, B. The design and verification of MuMax3. *AIP. Adv.*, **2014**, 4(10), 107133.
42. Leliaert, J.; Dvornik, M.; Mulkers, J.; De Clercq, J.; Milošević, M.V.; Van Waeyenberge, B. Fast micromagnetic simulations on GPU—recent advances made with MuMax3. *J. Phys. D: Appl. Phys.*, **2018**, 51(12), 123002.
43. Je, S.G.; Thian, D.; Chen, X.; Huang, L.; Jung, D.H.; Chao, W.; Lee, K.S.; Hong, J.I.; Soumyanarayanan, A.; Im, M.Y. Targeted Writing and Deleting of Magnetic Skyrmions in Two-Terminal Nanowire Devices. *Nano Lett*, **2021**, 21(3), 1253.
44. Koshibae, W.; Kaneko, Y.; Iwasaki, J.; Kawasaki, M.; Tokura, Y.; Nagaosa, N. Memory functions of magnetic skyrmions. *Jpn. J. Appl. Phys.*, **2015**, 54(5), 053001.

45. Zhang, X.C.; Xia, J.; Zhao, G.P.; Liu, X.X.; Zhou, Y. Magnetic skyrmion transport in a nanotrack with spatially varying damping and non-adiabatic torque. *IEEE Trans. Magn.*, **2017**, 53(3), 1500206.
46. Chen, X.; Kang, W.; Zhu, D.; Zhang, X.; Lei, N.; Zhang, Y.; Zhou, Y.; Zhao, W. Skyrmion dynamics in width-varying nanotracks and implications for skyrmionic applications. *Appl. Phys. Lett.*, **2017**, 111(20), 202406.
47. Zhang, X.; Zhao, G.P.; Fangohr, H.; Liu, J.P.; Xia, W.X.; Xia, J.; Morvan, F.J. Skyrmion-skyrmion and skyrmion-edge repulsions in skyrmion-based racetrack memory. *Sci Rep*, **2015**, 5, 7643.
48. Gorshkov, I.O.; Gorev, R.V.; Sapozhnikov, M.V.; Udalov, O.G. DMI-gradient-driven skyrmion motion. *ACS Appl. Electron. Mater.*, **2022**, 4(7), 3205.